Proceedings of the 8th International Symposium
on Experimental and Computational
Aerothermodynamics of Internal Flows
Lyon, July 2007
Paper reference : ISAIF8-00131

Particle Image Velocimetry of Turbulent Mixed Convection at Ambient and High Pressure

[1]**N. Grabinski,** [1]**A. Westhoff,** [1]**J.Bosbach,** [2]**A. Thess and** [1]**C. Wagner**

1 - Institute of Aerodynamics and Flow Technology, German Aerospace Center (DLR), Bunsenstr. 10, D-37073 Göttingen

2 - Ilmenau University of Technology, Department of Mechanical Engineering, P.O. Box 100565, D-98684 Ilmenau

Measurement of turbulent mixed convection at reduced model size by aerodynamic scaling is a promising approach to simplify the investigation of many technical configurations and offers the potential to make large scale flows accessible on a laboratory scale. On the pathway to measurement of turbulent mixed convection at high pressure by Particle Image Velocimetry forced, free and mixed convection have been investigated in a generic convection cell at ambient pressure. The scaling theory, which allows to down scale the cell, is presented, the PIV set up used for measurement at high pressure conditions in the high pressure wind tunnel in Göttingen is discussed, and the cell, which is capable of being operated at high pressure, is reviewed. Finally, first results of measurements at ambient pressure in a closed loop open test section wind tunnel at $Re = 3500$, $Gr = 9 \cdot 10^5$, $Pr = 0.7$ and $Ar = 0.4$ are discussed.

Keywords: Rayleigh number, Reynolds number, Prandtl number, Grashof number, Archimedes number, free convection, forced convection, mixed convection, aerodynamic scaling

Introduction

The superposition of forced and free convection is called mixed convection. It is characterized by the Archimedes number $Ar = \sqrt{Gr} / \mathrm{Re}$, i. e. the ratio of buoyancy and inertia forces, the Reynolds number *Re* and the Prandtl number *Pr*. *Gr* denotes the Grashof-number and reflects the impact of buoyancy on the flow. For very small *Ar* the flow is governed by inertia forces, while at very high *Ar* buoyancy forces dominate. In the intermediate region of *Ar* the flow field depends on both, buoyancy and inertia forces. This regime is referred to as mixed convection which occurs in many technical applications like e.g. heat exchangers [12, 13] or air conditioning in passenger compartments [3]. Moreover, mixed convection is an often occurring phenomenon in geology and meteorology. Since many of these flow situations involve large scales, acquiring such flows experimentally at full scale can be difficult. As a consequence a measurement method which allows for investigation of large scale mixed convection at a reduced model size is highly desirable. The approach of our experiment is to reduce the spatial dimensions of such configurations to scales which are experimentally accessible by increasing the fluid pressure and the inflow velocity and thus keeping *Gr*, *Re*, *Pr* and thereby *Ar* constant.

There are several studies considering mixed convection in different configurations and using various measurement techniques and parameter ranges. A configuration often chosen for these studies is mixed convection between two horizontal plates cooled from above and heated from below. You et al. [15] measured mixed convection for $3530 < Gr < 1.18 \cdot 10^4$ and $15 < Re < 150$ with Laser-Doppler anemometry. Baskaya et al. [2] investigated the impact of buoyancy forces on the local

Nusselt number for $241 \leq Re \leq 980$ and $9.53 \cdot 10^5 \leq Gr \leq 1.53 \cdot 10^7$ in a horizontal channel, which was equipped with an array of discrete heat sources at the bottom. Costa [6] investigated mixed convection of a hot air jet with two-component Laser-Doppler anemometry. Other investigations, which deal with flows in rectangular cells, were considered for different boundary conditions and aspect ratios by Shankar et al. [11] and for a vertical rectangular duct with a Gr/Re ratio of up to 600 and several aspect ratios by Barletta et al. [1].

Closely connected to our study are also measurements of Rayleigh-Bénard convection (RB) at high Rayleigh numbers using different pressurized gases as fluid. For example, Fleischer and Goldstein [8] worked with Rayleigh numbers up to $Ra = 1.7 \cdot 10^{12}$, whereas Niemela [13] examined the scaling of the Nusselt with the Rayleigh number in RB for Ra up to 10^{17} [9].

However, to our knowledge, measurement of mixed convection at high fluid pressure, particularly by means of PIV, has not been performed so far.

At the German Aerospace Centre in Göttingen a modularly designed convection cell was developed allowing to study mixed convection in a range of $600 < Re < 3 \cdot 10^6$, $5 \cdot 10^5 < Gr < 5 \cdot 10^{10}$ and thus for Ar from nearly 0 up to 370 with air as working fluid. In order to cover this range the cell was enabled to operate within a pressure range of $1 < p < 100$ bar. The aim is to apply PIV at high pressure in order to study the influence of buoyancy on the forced convection at high Grashof and Reynolds numbers considering the concept of a scaling theory.

Here, first results of the flow in the convection cell at ambient pressure obtained by Particle Image Velocimetry are reported. Results at elevated fluid pressure up to 10 bar will be obtained in the near future. For this the cell will be operated in the HDG (High Pressure Wind Tunnel Göttingen).

Scaling theory

Mixed convection in a given geometry is characterised by three independent nondimensional parameters, namely

$$Gr = g\alpha\Delta T H^3/\nu^2, \quad (1)$$

$$Re = UL/\nu \quad (2)$$

$$\text{and } Pr = \nu/\kappa, \quad (3)$$

where g denotes the gravitational acceleration, H the height of the cell, $\alpha = -1/\rho\,(\partial\rho/\partial T)$ the thermal expansion coefficient, υ the kinematic viscosity, κ the thermal diffusivity, U the inlet velocity, and L the characteristic length scale of the system. Often one would like to study the flow with the same nondimensional parameters but in a geometry whose size H' is by a factor s smaller than its original size, i.e. $H'=s_H H$. Scaling theory tells us how one has to scale velocity, viscosity, thermal diffusivity, and the thermal expansion coefficient in order to accomplish this task. Assuming that the thermal expansion coefficients is independent of pressure for our working fluid air one can readily verify that the scaling coefficients for the mentioned quantities are related to s by the relations

$$Gr = g\alpha\Delta T(s_H H)^3/(s_\nu \nu)^2, \quad (4)$$

$$Re = s_U U s_L L/s_\nu \nu \quad (5)$$

$$\text{and } Pr = s_\nu \nu/s_\kappa \kappa, \quad (6)$$

The corresponding scaling factors are denoted as s_i. Under the constraint of geometrical similarity, i.e. $s_L = s_H$, we obtain the two equations

$$s_\nu = (s_H)^{3/2} \text{ and } s_U = (s_H)^{1/2}. \quad (7)$$

Scaling of the system by a factor s_H for the height of the container yields the scaling factors for kinematic viscosity s_ν and the inflow velocity s_U. Since μ, the dynamic viscosity, is unaffected by the pressure in the regime of 1 bar $< p <$ 20 bar, the kinematic viscosity can be controlled via the density ρ, which in turn depends on the pressure p linearly for air. This allows to compare a large scale system to a downscaled system by increasing the pressure and adjusting the inflow velocity.

Experimental Setup

Convection cell

Our convection cell consists of a cuboidal container with a quadratic cross section, an air inlet at the top and an air outlet at the bottom. The cell has a width of 0.1 m, a height of 0.1 m and a length of 0.5 m. Different in- and outlet configurations have been considered in our measurements. In the first configuration (configuration I, Fig. 1a) the in- and outlet are located at the same side of the cell, while in the second configuration (configuration II, Fig. 1b) the in- and outlet are placed on opposite sides of the cell. Both, air in- and outlet, span the whole length of the cell and are constituted by rectangular channels with a channel height of 5 mm and a length of 200 mm for the inlet and a channel height of 10mm and a length of 120 mm for the outlet. The inlet channel is equipped with an additional fence in order to further homogenize the inflow.

All side walls are thermally insulated by a layer system with an insulating sheath of 7 mm air between two layers of transparent windows in order to get nearly adiabatic boundary conditions while maintaining the optical accessibility of the cell.

For both configurations the floor of the container is equipped with a heated cooper plate and the ceiling with an aluminum heat exchanger. Cooling is realized by cooling fins, which provide thermal coupling between the cooling plate and the air in the wind tunnel.

Resistance Temperature Detectors (RTDs) are embedded in the cooling and heating plate (see Fig. 1a) in order to monitor the temperatures of our cell. Both, ceiling and floor of the cell are equipped with eight RTDs each in configuration I. Further the in- and outflow temperature are recorded with RTDs. In configuration II the cell was equipped with four RTDs, i.e. one at the heating plate, one at the cooling plate, one in the inlet and one in the outlet.

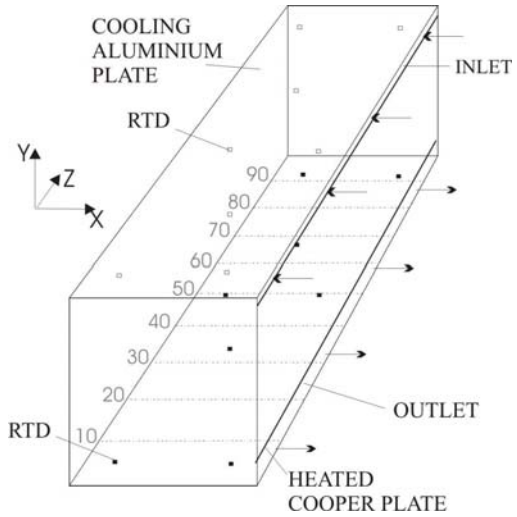

Fig. 1a Sketch of the convection cell in configuration I with heated copper plate at the bottom, cooling aluminum plate at the top, inlet, outlet and embedded RTDs (black in heating, white in cooling plate). The light sheet levels (10 to 90 percent of length) are marked on the floor.

With these configurations we are able to generate well defined mixed convection in two different ways. In configuration I the incoming air enters the cell through the inlet at the top, follows the ceiling and the sidewall at the opposite side and finally flows over the heating plate (not shown). In this case the mean wind divides in two parts: One part follows the left sidewall back to the inlet and the other one exits the cell through the outlet. For configuration II the incoming air enters the cell through the inlet and follows the ceiling and the opposite sidewall as well, but then splits into two parts as presented in Fig. 4 and Fig. 5: One main part, which exits the cell through the outlet and a second part, which flows back to the inlet over the heating plate. In both configurations the mean wind rotates in opposite clockwise direction, its center being located, depending on the *Ar* and *Re* number, close to the cell core.

The measurements at ambient pressure were performed in the open test section of a closed loop wind tunnel, which allows for free stream velocities up to 65 m/s. The flow in the tunnel provides homogeneous inflow conditions for our air inlet. Furthermore it serves as a heat sink for our cooling plate. This configuration has been preferred over a simple fan, because it enables us to test the flow behavior in our cell under similar conditions as in the high pressure wind tunnel.

Particle Image Velocimetry set up

Particle Image Velocimetry (PIV) has been applied in order to measure mixed convection in our cell.

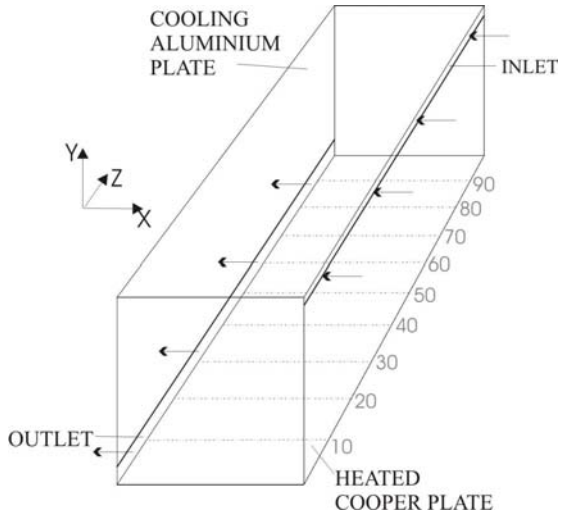

Fig. 1b Sketch of the convection cell with heated copper plate at the bottom, cooling aluminum plate at the top, inlet and outlet at the opposite side. The light sheet levels (10 to 90 percent of length) are marked on the floor.

The PIV system consists of a double oscillator quality switched Nd:YAG laser, a light sheet optic and a Peltier-cooled charge coupled device (CCD) camera (1376×1040 spatial resolution at 12 bit grayscale), which is placed in front of the convection cell. The light sheet is injected into the cell from the opposite side of the air inlet and can be traversed in the longitudinal direction (z). According to the optical set up only the velocity components in the light sheet plane were detected (2C-2D PIV). Depending on the fluid pressure different kinds of seeding particles are used for PIV. For measurement at ambient pressure small droplets of Di-Ethyl-Hexyl-Sebacat (DEHS) with a mean diameter of 1µm generated with a Laskin nozzle generator have been used. For measurements at elevated pressure solid Matroxid (Al_2O_3) particles as well as Expancel micro spheres (511DE20d60', small spherical plastic particles with a size of 18 -28 µm) will be used as discussed in the following.

High pressure wind tunnel Göttingen (HDG)

The measurement at high pressure will be performed in the HDG, which is a Göttinger-type closed circuit low speed wind tunnel and can be pressurized up to 100 bar (Fig. 2). The velocity is adjustable between 3.5 and 35 m/s in the total range of pressure. At a temperature of 300 K with the standard reference length definition of 0.06 m, the Reynolds number can be varied up to $1.2 \cdot 10^7$. The test section has a height of 0.6 m, a width of 0.6 m and a length of 1 m.

At high fluid pressure the choice of the seeding in a PIV measurement is of particular importance, since the particles bear the risk of dust explosion. As mentioned before we plan to use Expancel micro spheres (`511DE20d60`) as well as solid Matroxid (AL_2O_3) particles. Matroxid, being chemically very inert, is uncritical concerning dust explosions as opposed to the Expancel particles.

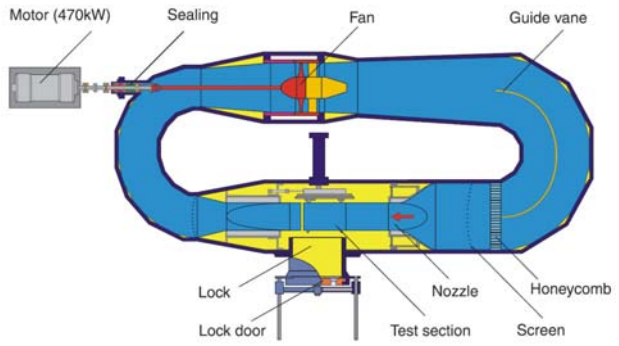

Fig. 2 Sketch of the High Pressure Wind Tunnel Göttingen (HDG).

There are several characteristics, which define the inflammability and explosiveness of solid substances in air. The maximum explosion pressure P_{max} is the maximum pressure which occurs in a dust explosion. The temporal derivation of P_{max} is the maximum rate of pressure rise (MPR)

$$MPR = \frac{dP}{dt} = AP_i^x + B\,, \tag{8}$$

where A, B and $0 < x < 1$ are empirical values depending on the substances and P_i the initial pressure [5]. The normalized pressure rise rate (K_{St} value) is given by

$$K_{St} = \frac{dP}{dt} V^{1/3} \tag{9}$$

The lower explosion limit (LEL) is the minimum mean concentration which is necessary for an explosive air dust mixture. It depends on the initial pressure.
The LEL usually increases with rising pressure as it has been shown e.g. for coal or polyethylene dust by Cashdollar, Conde Lazaro or Wiemann [4, 5, 14].

But the regime of mean concentration of Expancel (LEL 57 g/m^3 at ambient pressure), which is necessary for PIV in the HDG, is less than 1/10000 of the LEL. Furthermore the flow in the HDG is very homogeneous. In combination with the very good following behavior of the Expancel particles a rather homogeneous distribution of the seeding particles in the total volume of the wind tunnel can be expected. In summary there is an increase of LEL with rising pressure, a homogeneous distribution of particles and a very low mean concentration compared to the LEL. Hence the risk of dust explosion is negligible.

Measurement Conditions

In the following only results for cell configuration II are discussed. Three cases, i.e. free, forced and mixed convection have been investigated. The measurements presented here were conducted in the crosscut plane at 50 percent of the cell length (Z/2). As already mentioned air with Pr number $Pr = 0.7$ was used as working fluid. For forced and mixed convection the Re number, based on the width of the cell as characteristic length, was $Re = 3500$. A temperature difference of 7 K between heating and cooling plate resulted in a Gr number of $Gr = 9 \cdot 10^5$ for free and mixed convection. As a consequence the Ar number for mixed convection amounted to $Ar = 0.4$.

The velocity maps in the measurement plane were recorded in 4 series of 160 double images at a repetition rate of 4 Hz. From these 640 instantaneous 2C-2D velocity maps the average as well as the root mean square of the deviations from the average (RMS) has been calculated. Along with the in-plane velocity vectors the 2C velocity magnitude $W = (U^2 + V^2)^{1/2}$ of the flow field is depicted in the plots. The x- and y-coordinates were made dimensionless by division with the height of the cell. The z-coordinate was made dimensionless by division with the length of the cell.
The velocity of the flow field is depicted by vectors with the length of the in-plane velocity magnitude. For the sake of visibility only every second vector is plotted in each direction. The RMS values are presented as contour lines with levels between 0 and 10.

The black bar at the lower region of the velocity maps is the result of light sheet blockage by the outlet.

Results and discussion

Averaged velocity field

Figure 3a depicts the average velocity map for free convection. As can be seen clearly, the mean flow is di-

rected downwards in the measurement plane. Furthermore small vortices occur in the lower left and right corners, rotating in opposite directions. The mean velocity map can be divided into 4 regions: First there is a region between Y = 0.9 and Y = 1 with a rather low velocity. The broadest region is the second one, where the downward flow occurs (0.1 < Y < 0.9). Close to the bottom a narrow region of low-velocity is observed, which is bounded laterally by the two vortices in the lower corners of the cell.

The velocity map for the case of forced convection in Fig. 4a reflects a jet of incoming air from the inlet. Initially it follows the ceiling, but detaches at X = 0.3 in order to flow downward at the left sidewall and leave the cell through the outlet. As a consequence a roll structure is generated, which rotates in opposite clockwise direction, its core being located in the center of the cross section. Due to the separation, vortices at the upper left and the lower right corner can be observed.

Finally in Fig. 5a the time averaged velocity map for the case of mixed convection is presented. Similarly as in the case of forced convection the mean flow enters the cell through the inlet, follows the ceiling but detaches later. Further, a roll structure rotating in opposite clockwise direction is generated as well, but in contrast to forced convection the magnitude of gyration is increased drastically. With the onset of buoyancy the center of the roll is shifted to the lower right corner. The recirculating part of the jet separates from the side wall prior to recombination with the incoming air jet, resulting in a large vortex in the inlet region. In addition two more vortices can be observed in the upper left and lower right corner of the cell.

Statistical quantities of the velocity maps

Figure 3b, 4b and 5b depict the maps of RMS values for the case of free, forced and mixed convection, respectively. For free convection (Fig. 3b) the velocity fluctuations are of the same order of magnitude as the mean velocity, which is due to the fact that the flow field is strongly influenced by the intermittent emission of thermal plumes from the bottom. This is revealed by the instantaneous velocity maps, see e.g. Fig. 6. Clearly a main downward flow from the upper region is reflected, which hits a rising plume in the center of the lower part of the cross section. Due to the collision of rising and falling plumes the RMS values are increased in the lower quarter of the cross section. This was also observed by Xia et al. [16] or Krishnamurti and Howard [8] in a cubic closed box with water as working fluid.

In the case of forced convection the highest velocity fluctuations occur in the region of the jet (see Fig. 4b), where the RMS values amount up to 30 percent of the maximum velocity magnitude. We would like to mention, that the RMS values in the upper region of the side walls are the result of background reflections in the PIV measurement. In the region of the rotating mean wind the RMS values are quite low and amount to less than 10 percent of the maximum velocity magnitude, indicating a rather stationary behavior of the roll structure.

The contour map of the RMS values for the case of mixed convection clearly reveals the influence of buoyancy forces on the velocity fluctuations. It can be recognized that the RMS values are drastically increased particularly in the jet region. The enhancement in this region amounts to about a factor of two. Furthermore the area with fluctuations of 10 and more percent of the maximum velocity magnitude grows. Even though an area of increased RMS values is generated close to the core of the cell due to thermal convection the velocity fluctuations remain lower than 10 percent of the maximal velocity magnitude in the major part of the cross section. Additionally a dramatic increase of RMS values above the heating plate particularly close to the outlet can be detected. Again, the increased RMS values at the upper left and right side are due to background reflections of the laser light.

Jet broadening and center shifting

As already mentioned with the onset of mixed convection two essential effects occur: The first is the broadening of the inflow jet and the second the shifting of the rotation center. These two effects will be discussed in the following starting with the jet broadening.

The reason for the broadening is revealed by the instantaneous velocity fields of mixed convection, see e.g. Fig. 7. Approximately at X/2 a rising plume can be observed, which hits the jet at the ceiling prior to its deflection to the left by the jet. As a result the jet is broadened and the average of the roll velocity increases.

In order to further analyze the jet and roll structure line scans of the U and V velocity and RMS components have been calculated, see Fig. 8a – 8d.

The change of the roll structure upon the onset of mixed convection can be detected nicely in the line scan of the V-velocity component at Y/2 (see Fig. 8a).

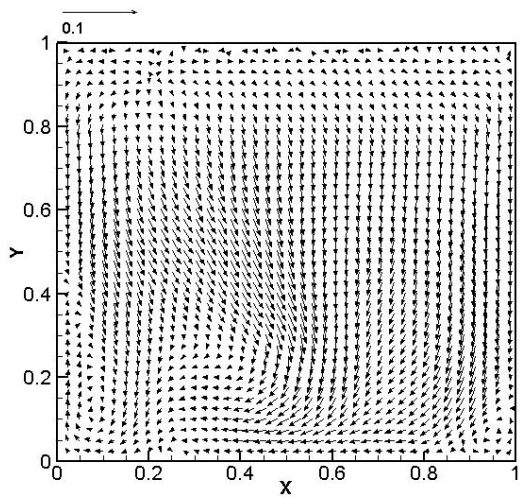

Fig. 3a Time-averaged in-plane velocity maps at Z/2 of free convection with $Gr = 9 \cdot 10^5$.

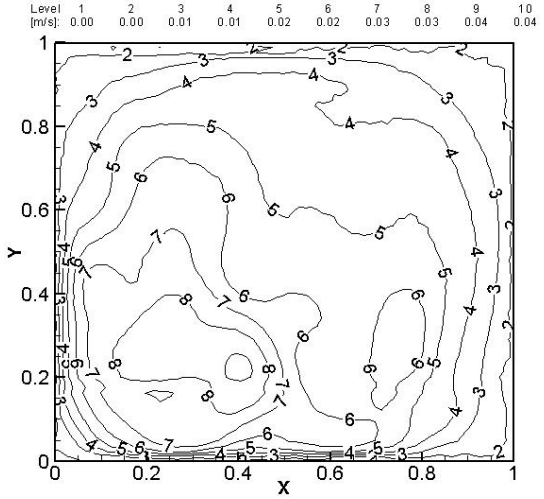

Fig. 3b RMS values of the velocity fluctuations corresponding to the results of Fig. 3a.

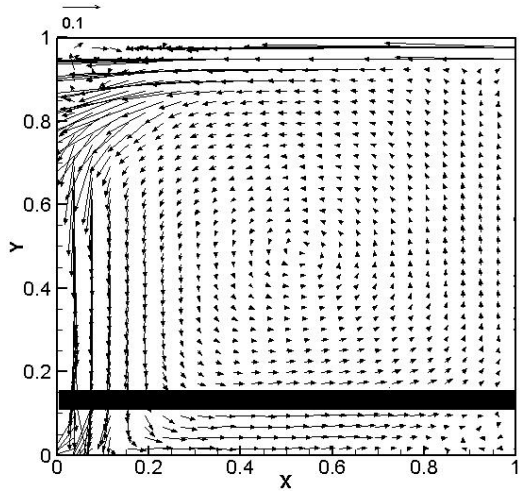

Fig. 4a Time-averaged in-plane velocity magnitude for configuration II at Z/2 for forced convection with $Re = 3500$.

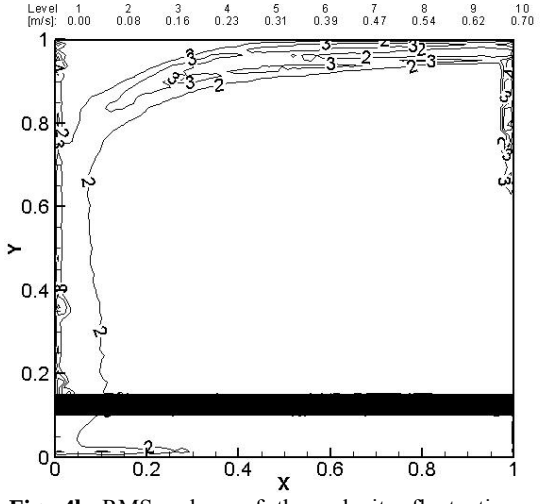

Fig. 4b RMS values of the velocity fluctuations corresponding to the results of Fig. 4a.

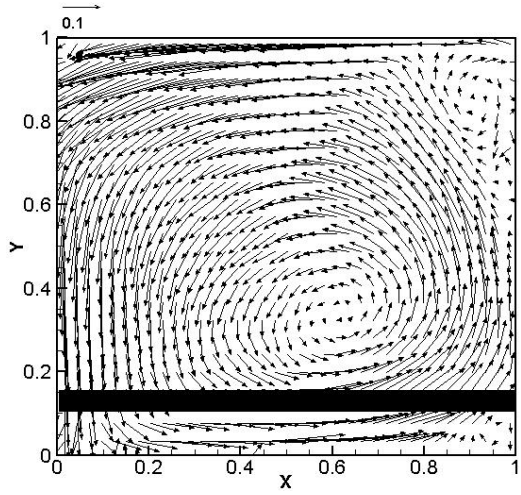

Fig. 5a Time-averaged in-plane velocity magnitude for configuration II at Z/2 of mixed convection.

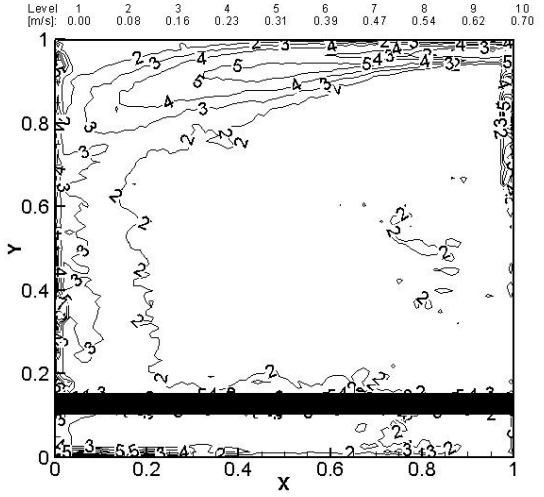

Fig. 5b RMS values of the velocity fluctuations corresponding to the results of Fig. 5a.

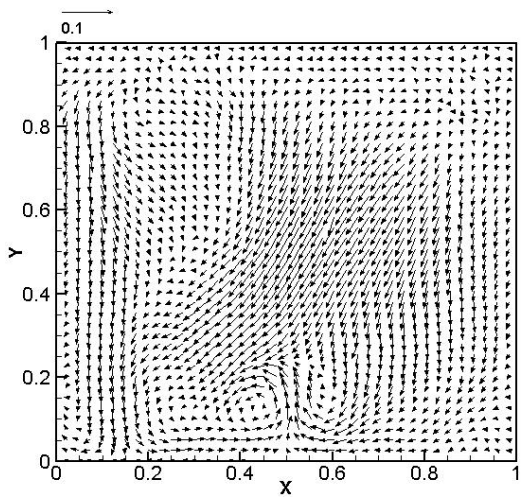

Fig. 6 Instantaneous velocity magnitude at Z/2 of free convection with $Gr = 9 \cdot 10^5$.

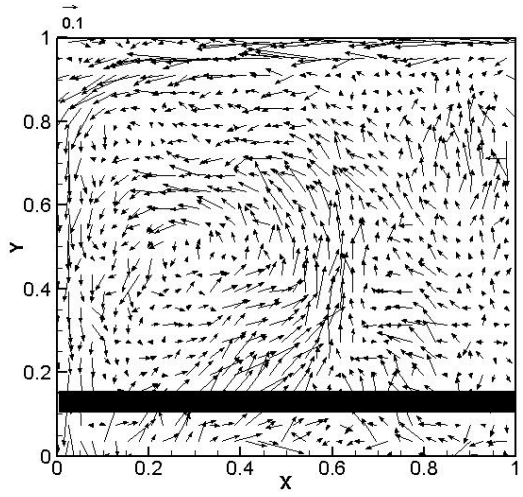

Fig. 7a Instantaneous in-plane velocity magnitude for configuration II at Z/2 of mixed convection with $Gr = 9 \cdot 10^5$, $Re = 3500$ and thus $Ar = 0.4$.

In the case of forced convection the downward directed part of the roll at the left side is primarily located between $0 < X < 0.1$ and exhibits a maximum velocity of 0.33 m/s. For mixed convection the maximum velocity decreases to 0.28 m/s, but the roll becomes broadened. Also a strong increase of the V-component at the right side can be observed. Finally for the case of mixed convection the shift of the roll center is reflected by a shift of the zero crossing of the V-component in comparison to forced convection.

The line scans of the U component at Y/2 of the time-averaged velocity maps (Fig. 8b) reveal the extreme rise of the U velocity component in the case of mixed convection. Furthermore it can be seen that the minimum of the U-component is shifted to larger X values, reflecting the shift of the roll center to the lower right.

In the line scans Fig. 8c and 8d the corresponding RMS values of the velocity components at Y/2 are presented. Due to the interaction of intermittent thermal plumes and the roll the RMS values of the V-component are significantly enhanced for mixed convection, although the maximum velocity magnitude is decreased, see Fig. 8c. The strength of the velocity fluctuations is almost equal to the velocity magnitude itself for mixed convection. The same holds for the U-component, presented in Fig. 8d.

Finally we would like to note, that with other ratios of inflow velocity and temperature difference the center of the role will shift to the lower left side (not shown here). As the PIV measurements disclose the shift to the left side increases with rising *Ar* number.

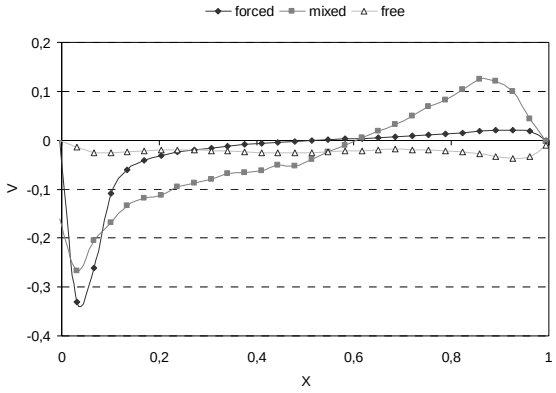

Fig. 8a Line profile of the time-averaged V-component Y/2 for free (triangle), forced (diamond) and mixed (square).

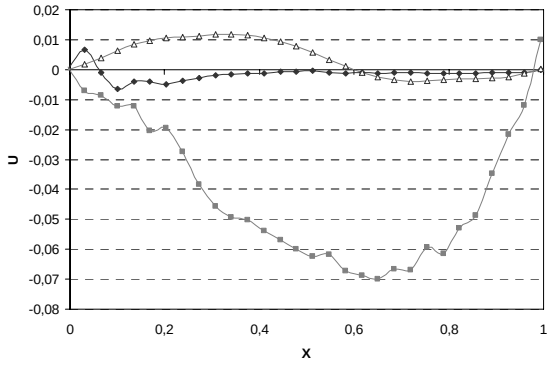

Fig. 8b Line profile of the time-averaged U-component at Y/2 for free (triangle), forced (diamond) and mixed (square).

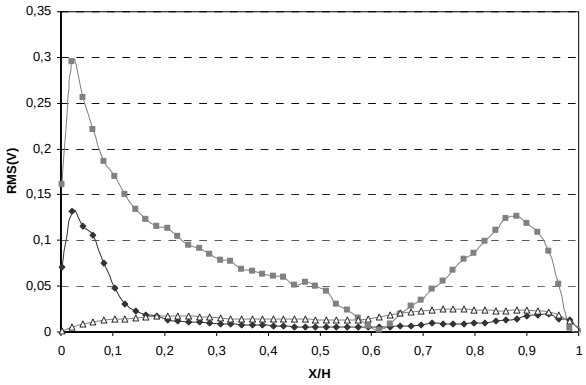

Fig 8c The RMS values of the velocity fluctuations for the V- component at Y/2.

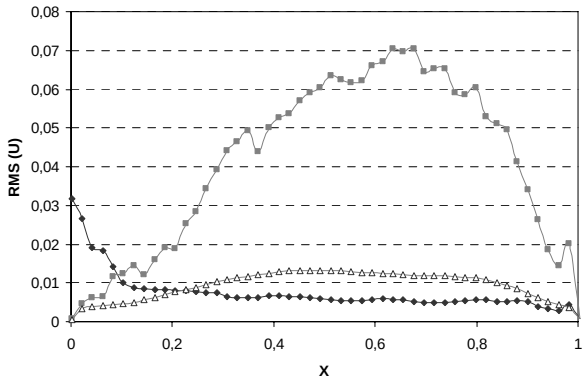

Fig 8d The RMS values of the velocity fluctuations for the U- component at Y/2.

Summary and conclusion

Forced, free and mixed convection have been investigated in a rectangular convection cell at ambient pressure by Particle Image Velocimetry. A scaling theory, which allows to down scale the cell, has been presented. The convection cell, which is capable of being operated at high pressure, was reviewed. First results of measurements at ambient pressure in a closed loop open test section wind tunnel at $Re = 3500$, $Gr = 9 \cdot 10^5$, $Pr = 0.7$ and $Ar = 0.4$ were discussed in detail. For the three scenarios of convection time-averaged velocity fields as well as the corresponding RMS maps of the velocity fluctuations have been presented.

Two main regions of flow field are identified: (1) A central opposite clockwise rotating core; (2) a jet entering the inlet at the upper right side following the ceiling, the left sidewall and leaving the cell through the outlet. By comparing the three cases of convection to mixed convection the following findings have been made: (1) a jet broadening (2) a shifting of the core of the roll (3) a velocity increase of the rotating velocity and (4) a strong increase of the velocity fluctuations.

In addition instantaneous velocity maps for the cases of free and mixed convection exposed the interaction of intermittent thermal plumes with the mean wind.

In the near future forced and mixed convection in our cell (configuration I) will be investigated in the HDG at elevated pressure up to 20 bar in order to analyze the influence of high *Re* and *Gr* numbers on the flow and to prove the scaling theory. The obtained results will be presented at the conference.

Acknowledgment

We are grateful to the Helmholtz society for financially supporting the present work with the grant ‘Virtual Institute for Thermal Convection’.

References

[1] Barletta, A., Di Schio, E. R., and Zanchini, E.: Combined forced and free flow in a vertical rectangular duct with prescribed wall heat flux, Int. Journal of Heat and Mass Transfer, vol. 24, pp.674-887, (2003).

[2] Baskaya, S., Erturhan, U., and Sivrioglu, M.: Experimental investigation of mixed convection from an array of discrete heat sources at the bottom of a horizontal channel, Heat Mass Transfer, vol. 42, pp.56-63, (2005).

[3] J. Bosbach, M. Kühn, C. Wagner, M. Raffel, C. Resagk, R. du Puits, and A. Thess: Large-scale particle image velocimetry of natural and mixed convection. In 13th Int. Symp. on Applications of Laser Techniques to Fluid Mechanics, Lisbon, Portugal, (2006).

[4] Cashdollar, K.L.: Coal dust explosibility, Journal of Loss Prevention in the Process Insustries, vol. 9, pp.65-76, (1996).

[5] Conde Lazaro, W., Garcia Torrent, J.: Experimental research on explosibility at high initial pressure of combustible dust, Journal of Loss Prevention in the Process Industries, vol. 13, pp.221-228, (2000).

[6] Costa, J. J., Oliveira, L. A., and Blay, D.: Test of several versions for the κ-ε turbulence modeling of internal mixed convection flows, Int. Journal of Heat and Mass Transfer, vol. 42, pp.4391-4409, (1999).

[7] Fleischer, A.S. and Goldstein, R.J.: High Rayleigh number convection of pressurized gases in a horizontal enclosure, Journal Fluid Mech., vol. 469, pp.1-12, (2002).

[8] Krishnamurti R. and Howard L.N.: Proc. Natl. A Ad. Sci. USA 78, (1981)

[9] Niemela, J. J., Skrebek, L., and Donnelly, R.: Turbulent convection at very high rayleigh numbers, Nature, vol. 404, pp.837-840, (2006).

[10] Raffel, M., Willert, C. E., and Kompenhans, J.: Particle image velocimetry – a practical guide, Springer Verlag, (1999).

[11] Shankar, P.N., Meleshko, V. V., and Nikiforovich, E. I.: Slow mixed convection in rectangular containers, Journal Fluid Mech., vol. 471, pp.203-217, (2002).

[12] Sillekens, J.J.M., Rindt, C.C.M. and Van Steenhoven, A.A.: Developing mixed convection in a coiled heat exchanger, Int. Journal of Heat and Mass Transfer, vol. 41, pp.61-72, (1998).

[13] Taylor, Francis: Mixed convection in a plane channel with a built-in triangular prism, Numerical Heat Transfer, vol. 39, pp.307-320, (2001).

[14] Wiemann, W.: Influence of temperature and pressure on the explosion characteristics of dust/air and dust/air/inert gas mixtures, Industrial Dust Explosion ASTM, vol. 958, pp.33-44, (1987).

[15] You, J., Yoo, J. Y., and Choi, H.: Direct numerical simulation of heated vertical air flow in fully developed turbulent mixed convection, Int. Journal of Heat and Mass Transfer, vol. 46, pp.1613-1627, (2002).

[16] Xia K., Sun C. and Zhou S.: Particle image velocimetry measurement of the velocity field in turbulent thermal convection, Phy. Rev., vol. 68, (2003).